Fabrication of CuO Pricky Microspheres with Tunable Size by a Simple Solution Route

Yanyan Xu, Dairong Chen,* and Xiuling Jiao

Department of Chemistry, Shandong University, Jinan 250100, People's Republic of China

Received: March 28, 2005; In Final Form: April 30, 2005

A simple aqueous solution route was introduced for the fabrication of CuO pricky microspheres (CPMs) using $CuCl_2 \cdot 2H_2O$, $Na_2(C_4H_4O_6) \cdot 3H_2O$ and NaOH as starting materials. The CPMs were composed of compressed nanothorns exhibiting tapering feature with tip size of less than 10 nm, and the size of CPMs could be tuned from 100−200 nm to 4−6 μm. The effects of the molar ratios of tartrate anions and NaOH to Cu^{2+} cations, reagent concentration, and reaction temperature on the products were investigated, showing that the morphology of CPMs was determined by the molar ratio of tartrate to Cu^{2+} cations and the size was greatly affected by reagent concentration and the molar ratio of NaOH to Cu^{2+} cations in the precursor solution. The fabrication of CPMs went through rapid nucleation of $Cu(OH)_2$, aggregation and in situ dehydration of $Cu(OH)_2$, oriented-aggregation-based growth, and normal crystal growth of CuO nanothorns. The nucleation and crystal growth were successfully separated by controlled releasing of Cu^{2+} and OH^- ions through the reversible reaction of Cu^{2+} cations, OH^-, and $C_4H_4O_6^{2-}$ anions.

I. Introduction

Hierarchical nano/microstructures, assemblies using nanoparticles, nanorods, nanobelts as building blocks,[1] and complex nanocrystals with well-defined shape and inner structure[2] have attracted great interests due to their novel properties and application convenience. In particular, the synthesis and analysis of hierarchical structures will facilitate deeper understanding of nature because there exist many kinds of organism with versatile architectures.[3] On the other hand, hierarchical superstructures or complex functional architectures offer opportunities in their novel collective properties, and they may be essential for building nanodevices with bottom-up approaches in the future.[1a−b,4] Recent research on sulfide semiconductor,[2a−b,4,5] transition metal oxide,[2d,6] and other nanostructures[7,8] has rapidly expanded into morphology/architecture-controlled synthesis.

As an important transition metal oxide with a narrow band gap (E_g = 1.2 eV), CuO, forms the basis of several high-temperature superconductors and giant magnetoresistance materials.[9] It is also a promising material for fabricating solar cells,[10] owing to its photoconductive and photochemical properties and lithium ion battery.[11] Therefore, the synthesis and fabrication of CuO nanomaterials have both fundamental and practical importance, and the nanostructured CuO materials and assemblies have attracted considerable attention in recent years. Up-to-date, well-defined CuO nanostructures with different morphologies such as nanoparticles, nanoellipsoids, nanoneedles, nanoshuttles, nanoleaves,[12] nanorods,[13] nanoribbons[14] and nanotubes[13b] have been synthesized successfully by a series of wet chemical methods in the presence of structure-directing surfactants or not. Besides radial CuO whisker arrays,[15] peanut-shaped nanoribbon bundle superstructures[16] and dandelion-like CuO hollow microspheres[17] have also been achieved through a microwave-induced polyol-processes, thermal decomposition of malachite precursor with similar morphology and solvothermal processes, respectively. Although great progresses have been made in the synthesis of CuO particles, hierarchical CuO architectures composed of nanoscale building blocks are seldom reported.

The solution methods have special advantages for the generation of hierarchical nanomaterials, but they are very complicated for nanostructures formed under such conditions experiencing nucleation, growth, aggregation, and Ostwald's ripening chemical processes.[18] Usually the precursor concentration changes continuously during crystal growth and aggregation; Ostwald's ripening and second nucleation often occur simultaneously, leading to the inhomogeneity of the particle size and morphology. In addition, the reactants are usually mixed one-off, and as reactants are consumed and byproducts generated, the solution's chemical environment, including solution components, pH values, and ionic strength, etc, changes greatly, bringing more variables to the nanomaterial formation. Many methods have been reported to overcome these drawbacks; however, the morphology control and fabrication mechanisms of hierarchical nanomaterials by the solution methods still remain great challenges. Herein, a system containing $CuCl_2 \cdot 2H_2O$, NaOH, and chelating agent sodium tartrate is designed to separate the nucleation and crystal growth by the control release of Cu^{2+} from $Cu(C_4H_2O_6)^{2-}$ anions. The nanostructured CPMs are prepared for the first time to our knowledge, and the formation mechanism of CPMs is investigated in detail. Compared with the previous reports, the present reversible reaction controlled synthetic process is simple, low-cost, and environmentally friendly without any organic solvents or organic structure-directing surfactants. Meanwhile, our results enrich the hierarchical CuO architecture family.

II. Experimental Section

Fabrication Procedures. All the reagents were of analytical-grade and were used without further purification. In the typical experiments, 1.42 mmol $CuCl_2 \cdot 2H_2O$ was dissolved in 30 mL deionized water to form a blue solution, and sodium tartrate was added into $CuCl_2 \cdot 2H_2O$ solution with the molar ratio of tartrate anions to Cu^{2+} (C_{R1}) of 1.15 to give a light bluish cupric

* Corresponding author. Telephone: +86-531-8364280; fax: +86-531-8364281; e-mail: cdr@sdu.edu.cn.

10.1021/jp051577b CCC: $30.25
Published on Web 06/25/2005

tartrate precipitate after stirring for several minutes. Into the mixture was added NaOH, in which the molar ratio of NaOH to Cu^{2+} (C_{R2}) was fixed in the range of 2.1−45.8 and the precipitate gradually dissolved, and a blue solution formed. Then the solution was heat-treated at 60−180 °C for 1−10 h to produce black precipitates (at 100 °C or below, water bath was used, and above 100 °C, hydrothermal reaction was carried out in Teflon-lined autoclaves of 40 mL capacity). After cooling to room temperature, the products were obtained by filtration, washed with deionized water and ethanol for several times, and finally dried in ambient environment.

Characterization Techniques. The morphology and microstructure of the products were characterized using a transmission electron microscope (TEM, JEM 100-CXII) with an accelerating voltage of 80 kV, a high-resolution transmission electron microscope (HRTEM, GEOL-2010) with an accelerating voltage of 200 kV, and a field-emission scanning electron microscope (FESEM, JEOL, JSM6700F). X-ray diffraction (XRD) patterns collected on a Rigaku D/Max 2200PC diffractometer with a graphite monochromator and CuKα radiation (λ = 0.15418 nm) were used to analyze the crystal structure of the products. Thermogravimetric analysis (TGA) was carried out on a METTLER to monitor the mass loss of CuO products at a heating rate of 10 °C·min^{-1} from 25 to 600 °C under air atmosphere. The infrared (IR) spectra were recorded on a Nicolet 5DX Fourier transform infrared (FT-IR) spectrometer using KBr pellet technique in the spectra range of 4000∼400 cm^{-1}. UV−vis absorption spectra were applied to track the variation of the solution during the whole process (UV−vis spectrometer, Lambda-35, Perkin-Elmer).

III. Results and Discussion

Morphology and Nanostructure of CPMs. The XRD pattern of a typical sample shown in Figure 1a indicates the formation of phase-pure monoclinic CuO crystallites (JCPDS file No.05-0661). The broadening of XRD lines results from the small size of nanothorns that composed the pricky spheres. The FE-SEM image (Figure 1b) shows that the size of CPMs is in the range of 4−6 μm, and the magnified FE-SEM image (Figure 1b inset) with well-defined pricky structure shows that the compressed nanothorns exhibit the tapering feature with tip size less than 10 nm. Furthermore, it also shows that the CPMs with the rugged surface (denoted with arrows) are not perfect spheres.

IR spectrum of CPMs gives adsorptions at 3393, 1623, 1395, 539, and 422 cm^{-1} (Figure 1c). The absorption at 3393 cm^{-1} can be attributed to the stretching vibration of absorbed H_2O or surface hydroxyls of the sample,[19] and the bands at 1623 and 1395 cm^{-1} are assigned to the asymmetrical stretching vibration and symmetrical stretching vibration of $RCOO^-$ absorbed on the CPMs surface, respectively.[20] The absorptions at 539 and 422 cm^{-1} are the characteristic stretching vibrations of Cu−O bond in monoclinic CuO.[21] The TGA curve shows a weight loss of ca. 2.5% from 120 to 550 °C, and there is no weight loss before 120 °C, indicating the absence of absorbed water in the products. Both the weight loss in TGA curve and the IR spectrum indicate the existence of surface hydroxyls and coordinated tartrate ions on CPMs.

Effects of the Reaction Conditions. To examine the function of tartrate anions in the fabrication of CPMs, the morphologies of the samples with different C_{R1} were compared. When no sodium tartrate was added, blue $Cu(OH)_2$ precipitated in the precursor solution, and only CuO sheets were obtained after heat-treated at 180 °C for 1 h. When C_{R1} was in the range of 0−0.5, in which the amount of tartrate anions was not enough

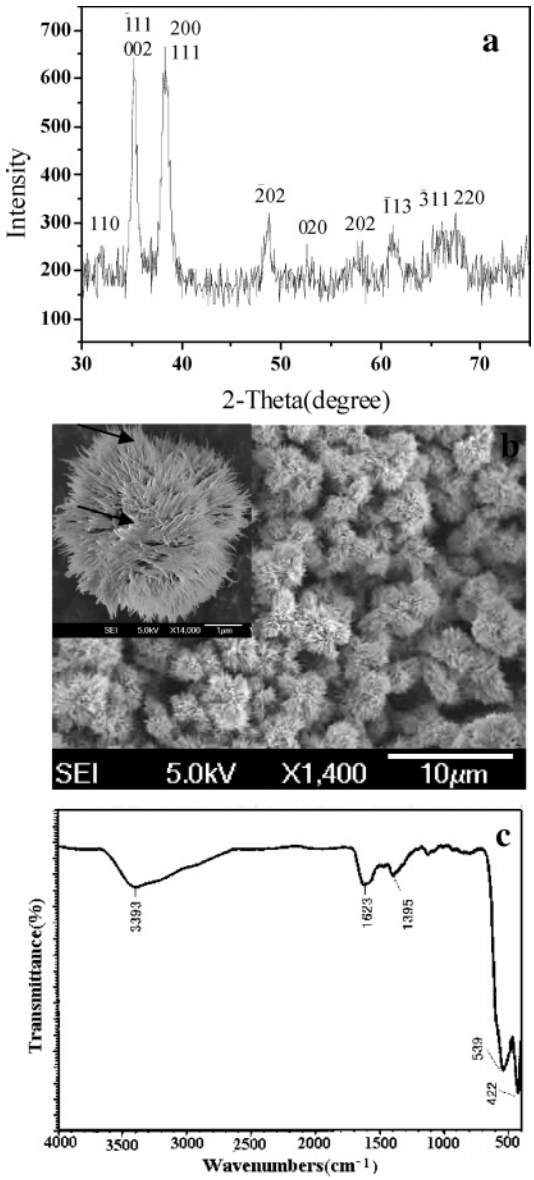

Figure 1. (a) XRD pattern, (b) FESEM images, and (c) IR spectrum of CPMs (No.1 in Table 1).

to form dissoluble complex, some CuO nanoflakes formed via direct dehydration of the colloid $Cu(OH)_2$ precipitate (Figure 2a). At the same time the compressed nanothorns with tapering feature (ca. 15 nm in diameter in tip end, 30 nm in diameter in root end and 300−400 nm in length) also precipitated due to the existence of tartrate anions (Figure 2b). With C_{R1} increasing the $Cu(OH)_2$ precipitate gradually decreased, and loosely flowerlike architectures composed of several nanobundles appeared when the solution was heated (Figure 2c). Finally, when C_{R1} exceeded 1, well-defined CPMs (Figure 1b) were formed. These results indicated that tartrate anions should be responsible for the formation of compressed nanothorns and the fabrication of CPMs.

To investigate the influence of NaOH on the products, the size of CPMs was compared with different C_{R2} while other conditions were kept constant, and the details were listed in Table 1. The results show that the size of CPMs decreased from 4−6 μm to 100−200 nm, with C_{R2} changing from 45.8 to 2.1 in the precursor solution (Figure 3). When C_{R2} was less than 2, it was difficult to obtain CuO. For example, no products formed after the solution (no. 7 in Table 1) was heat-treated at 180 °C for 4 h. Furthermore, diluting the precursor solution same as

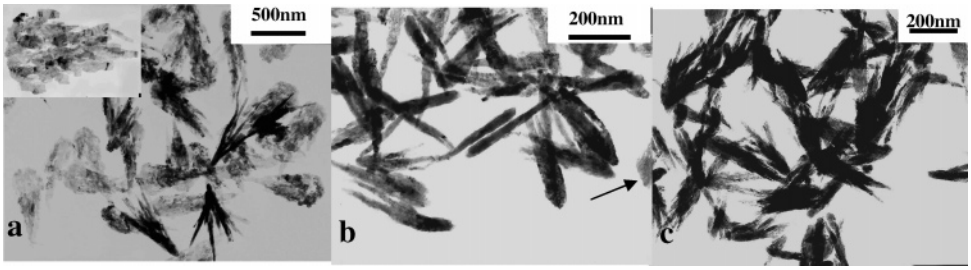

Figure 2. TEM images of CuO nanostructures obtained at different C_{R1}: (a) 0.10, (b) 0.26, and (c) 0.51. The concentrations of $CuCl_2 \cdot 2H_2O$ and NaOH are 0.047 and 2.15 mol·dm^{-3}, respectively; 180 °C for 1 h.

TABLE 1: The Diameter of CPMs Corresponding to Different C_{R2}[a]

no.	1	2	3	4	5	6	7
diameter (μm)	4−6	2.5−4	1−2	0.5−1	0.3−0.5	0.1−0.2	no products
C_{R2}	45.8	22.9	15.1	10.1	5.2	2.1	1.3

[a] The concentrations of $CuCl_2 \cdot 2H_2O$ and sodium tartrate are 0.047 and 0.054 mol·dm^{-3}, respectively. Temperature, 180 °C; time, 1 h.

no. 1 with equivalent deionized water while other conditions were held constant, the diameter of the compressed nanothorns and the aggregation degree did not markedly vary; only the size of CPMs decreased from 4−6 to 2−4 μm. Further decreasing the reagent concentration to one-third of the initial solution, the size of CPMs was 1−3 μm. Obviously, the size of CPMs significantly minished with the decreasing of reactant concentration and could also be controlled by adjusting C_{R2} in the precursor solution.

A series of experiments were conducted to investigate the necessary reaction temperature and time for the fabrication of CPMs. It was found that CPMs could be generated in a wide temperature range and 20−180 °C were chosen for convenience. As the reaction temperature decreased, the reaction time was obviously prolonged; for example, 1 h was enough to obtain CPMs at 180 °C, and 10 h and 1 month were needed at 60 and 20 °C, respectively. No significant change of morphology and size was observed. However, at higher temperature, Cu_2O impurity would be generated when reaction time was further prolonged, probably due to the deoxidization of tartrate anions. In summary, the increasing of reaction temperature accelerated the fabrication of CPMs, but the morphology and size of CPMs did not show significant change.

Fabrication Mechanism. To investigate the fabrication mechanism of CPMs, a detailed time course study as follows was conducted at 100 °C, while other reaction conditions were the same as no. 1 in Table 1. A spot of solution were taken from the system at different reaction times of 10, 13, 15, 18 min, cooled to room temperature rapidly and washed with deionized water. And UV−vis spectra were used to track the change of the solution during the reaction process.

After the solution was heated for 10min, the shuttle-like particles with length of 100−200 nm (Figure 4a) appeared, which were composed of parallel nanorods with the diameter of 8−12 nm and length similar to those of shuttle-like particles (Figure 4b). The lattice fringes image and SAED (selected area electron diffraction) pattern given in Figure 5a reveals that the nanorods were polycrystals composed of 4−5 nm clusters, and the calculated planar spaces of lattice fringes of 0.380 and 0.237 nm accorded well with the basal spacing computed for (021) and (041) planes in orthorhombic $Cu(OH)_2$, indicating $Cu(OH)_2$ intrinsic structure of those nanorods. Figure 4c shows that the self-assembling of $Cu(OH)_2$ shuttles occurred rapidly to form caltrop-like particles with their nanothorns composed of nanoshuttles. The corresponding XRD pattern confirms that the caltrop-like particles were phase-pure monoclinic CuO (Figure 6a), which revealed that accompanying the self-assembling of $Cu(OH)_2$ shuttles a rapid dehydration process existed. And along the oriented-assembling and growth of shuttle-like particles, the nanoclusters should also experience a process of orientation adjusting to share a crystallographic orientation with the dehydration to reach a lower energy level. With the reaction time prolonged, the primary pricky architectures gradually formed (Figure 4e), and the aggregates markedly enlarged. Figure 4f gives a magnified TEM image of a primary pricky architecture, which clearly shows that the compressed nanothorns were assembled from shuttle-like nanaoparticles. As reaction time further prolonging, the shuttle-like nanoparticles disappeared, and the pricky architectures as shown in Figure 4g formed, which was the rudiment of CPMs. The nanothorns resulted from oriented-aggregation-based growth were named as the truck nanothorns. The magnified TEM image (Figure 4h) indicated that the surface of the truck nanothorns was not smooth, and many voids were recognizable. The corresponding HRTEM lattice fringes image and SAED pattern (Figure 5b) confirmed the single-crystal nature of the truck nanothorns. On the basis of the planar space of lattice fringes calculated from Figure 5b, it is concluded that the truck nanothorn grew along the [010] direction (indicated with the arrow). Further prolonging the reaction time, the size of pricky architectures hardly changed, and many new branch nanothorns grew on the truck of rudiments. The density of branch nanothorns significantly increased with the reaction time prolonging, and the well-defined CPMs were formed at last. From 10−18 min, the aggregated nanostructures augmented almost in a magnification, and the particle size hardly changed in the following process. All the evidence indicated that the oriented-aggregation-based growth resulted in the formation of primary architectures of CPMs.

During the generation of CPMs, the solution also experienced great changes, which could be reflected by UV−vis absorption spectra. As shown in Figure 7, a strong absorption centered at ca. 670 nm was observed, which was assigned to d−d electron transfer of copper ions in complex form: $Cu(C_4H_2O_6)^{2-}$.[22] A largest adsorption (curve a) was given before nucleation. Curves b and c corresponded to the nucleation of $Cu(OH)_2$ and the following rapid aggregation, whose intensity showed only a slight decrease compared to curve a. However, the adsorption intensity significantly decreased in the after 15 min (curves d and e), which corresponded to the crystal growth stage. Further prolonging the reaction time to 1 h, the absorption curve was almost as same as curve e. The result indicates that the consume of the Cu^{2+} species centralized on the crystal growth stage, and ca. 40% of the initial Cu^{2+} species still existed in the solution as $Cu(C_4H_2O_6)^{2-}$ at the end of the reaction.

In the precursor solution, $Cu(C_4H_2O_6)^{2-}$ anions can form and a reversible reaction formulated as eq 1 exists, which prevents $Cu(OH)_2$ from precipitating.[23] With the temperature increasing,

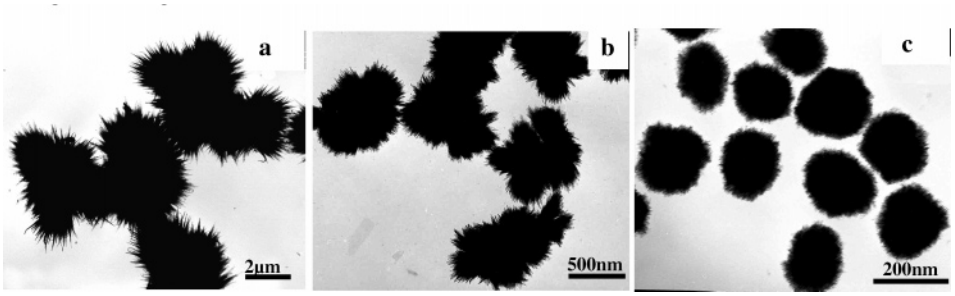

Figure 3. TEM graphs of the samples with different size: (a), (b), (c) was the products of no. 1, no. 4, and no. 6 in Table 1, respectively.

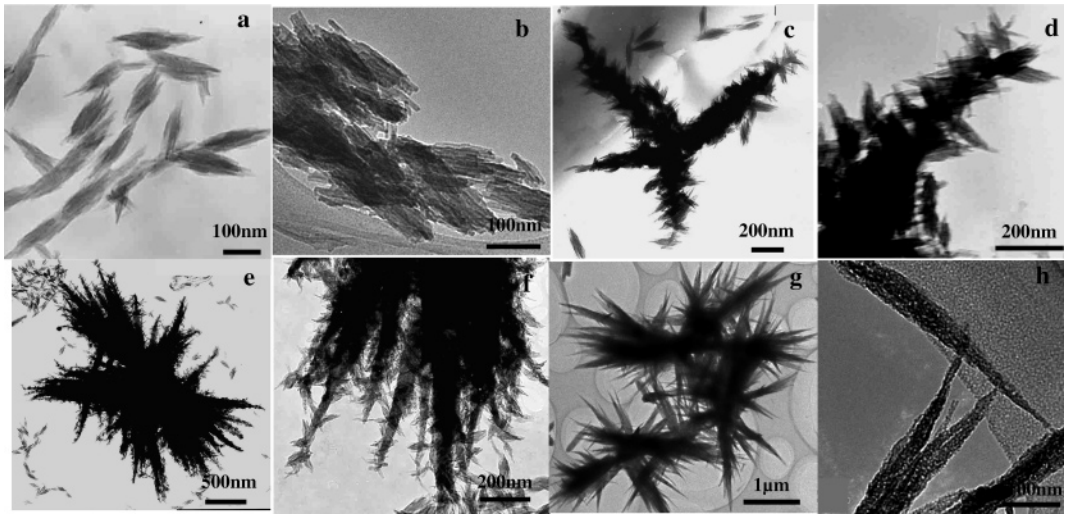

Figure 4. TEM images of samples taken at different reaction times. (a, b) 10, (c, d) 13, (e, f) 15, and (g, h) 18 min.

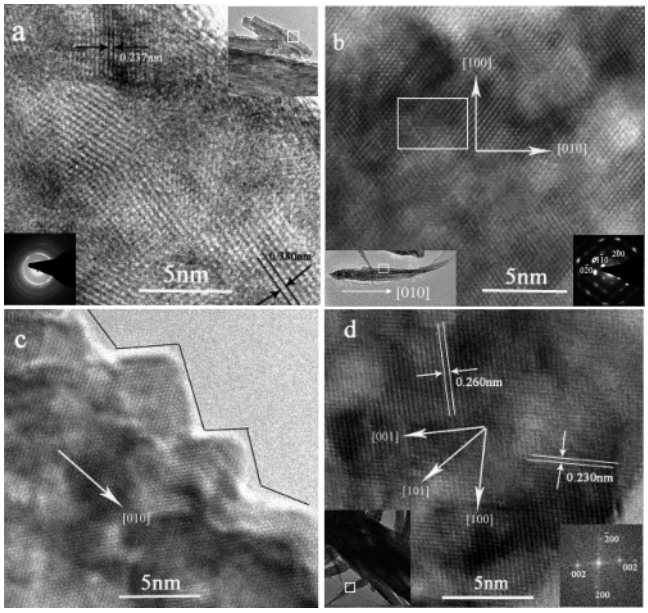

Figure 5. HRTEM graphs and corresponding selective area electron diffraction (SAED) of samples taken at reaction time of 10 (a) and 18 min (b−d).

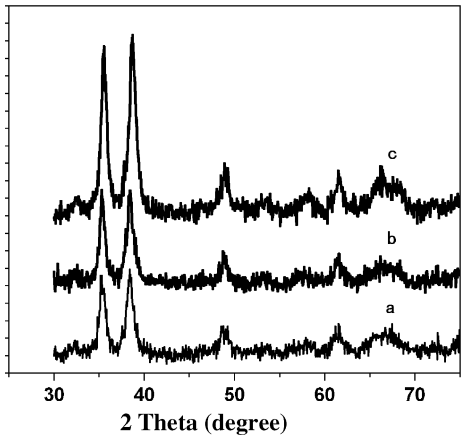

Figure 6. XRD patterns of the products after reacted at 100 °C for (a) 13, (b) 15, and (c) 18 min.

eq 1 would move toward right. Once the concentrations of Cu^{2+} cations and OH^- anions reached the critical nucleation concentration, a burst of homogeneous nucleation of $Cu(OH)_2$ occurred as expressed by eq 2, and a large amount of $Cu(OH)_2$ shuttle-like nanorods formed as shown in Figure 4a. The formation of $Cu(OH)_2$ relieved the supersaturation, at least rapidly enough to stop the nucleation due to the relative slower reaction rate of eq 1. The corresponding UV−vis spectrum indicates that only a small amount of Cu^{2+} species was consumed during the nucleation. And the in situ dehydration reaction as formulated in eq 3 rapidly carried out, accompanying by the atoms rearrangement to form CuO truck nanothorns as shown in Figure 4c,e,g. Compared to the nucleation of $Cu(OH)_2$, a relative lower supersaturation was required to heterogeneous growth (S_G) on CuO truck nanothorns surface, and the crystal growth rate was much faster than the releasing rate of Cu^{2+} cations from eq 1. So the concentration in the solution could not reach the necessary supersaturation (S_N) level to form $Cu(OH)_2$ nuclei for a second time, and the subsequent process exhibited the aggregated-growth and the normal crystal growth, which can be seen from the TEM observations. The aggregation-based growth resulted in many defects in the inner parts of a single nanothorn shown in Figure 5b (marked with square). At the same time, the steplike defects produced on the truck

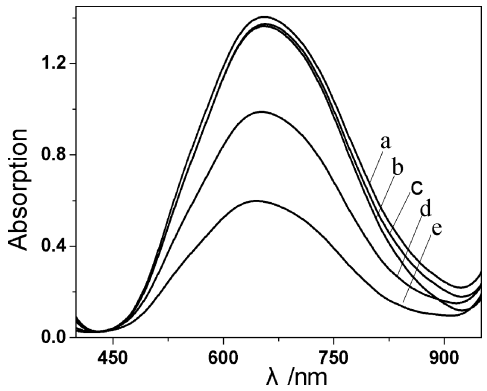

Figure 7. UV−vis absorption curves of reaction solution at different reaction time: (a) 5, (b) 10, (c) 15, (d) 20, and (e) 30 min. Water was used as the blank.

nanothorn surface (Figure 5c). HRTEM examination shows the "steps" appearing on the surface of almost every truck nanothorns, as well as on the center part of radical nanobundles. The higher surface energy of the steplike station than the tip of truck nanothorn might supply active sites for next crystal growth. So the constant supply of Cu^{2+} cations by eq 1 would facilitate further growth of CuO nanothorn along the surface steps by the arrangement of Cu^{2+} cations and oxygen atoms or OH^- anions. The supersaturation level was held at the range between S_N and S_G after the rapid formation of a large amount of $Cu(OH)_2$ nanoclusters, so the growth and nucleation steps were separated by controlled releasing of Cu^{2+} ions from copper-tartrate anions. UV−vis absorption analyses revealed that the consuming of Cu^{2+} species was centralized on the growth stage, and the remnants $Cu(C_4H_2O_6)^{2-}$ in the system at the end of reaction indicated that the reaction reached the equilibrium (eq 1,2) at this temperature, which revealed the reversible controlled reaction from the other point

$$Cu(C_4H_2O_6)^{2-} + 2H_2O \rightleftharpoons C_4H_4O_6^{2-} + 2OH^- + Cu^{2+} \quad (1)$$

$$Cu^{2+} + 2OH^- \rightleftharpoons Cu(OH)_2\downarrow \quad (2)$$

$$Cu(OH)_2 \rightarrow CuO + H_2O \quad (3)$$

The experiments revealed that the presence of tartrate anions was necessary for the oriented-aggregation based growth of CuO. In the process of oriented-aggregation, the single-crystalline nanothorns were formed through oriented arrangement by rotating adjacent nanoparticles to share an identical crystallographic orientation and then controlled removal of organic additives at interfaces.[24] On the basis of the calculation, the distances between the adjacent copper atoms on (100), (010), and (001) planes are respectively 3.083, 3.173, and 2.900 Å.[25] Thus, the tartrate anions preferred to selectively absorb on (010) plane due to its steric effect, which resulted in the oriented-aggregation of shuttles along [010] direction. As shown in eq 1, the increase of OH^- anions concentration would make the reaction moving toward left, which might result in more Cu^{2+} combination with tartrate anions. As a result, larger rudiments of CPMs were formed with the increasing of OH^- anion concentration.

As described above, except the oriented-aggregation growth mode, a normal crystal growth process also existed after nucleation. The oriented-aggregation growth was so fast that the steplike defects formed rapidly at the surface near the root of the compressed truck nanothorns (Figure 5c). Subsequently, the normal crystal growth at the steps started intermediately once the steps appeared. The surface energy of the nanothorns can be effectively lowered by the selective adsorption of tartrate anions to specific crystal structures, which results in the slow growth rate along this crystallographic plane in the normal crystal growth.[26] Thus, the (010) planes should exhibit a much slower growth rate during the normal crystal growth due to more capping molecules. In the present research, the compressed branch nanothorns grown from the step were observed by HRTEM, and Figure 5d gives a representative image. Calculation of the planer space of lattice fringes confirmed that the compressed branch nanothorn grew along the [101] direction, and the similar size in [100] and [001] direction was probably due to the similarity of atoms arrangement on (100) and (001) planes while the size of [010] direction was the shortest exhibiting as the thickness. In summary, there were two kinds of nanothorns in CPMs. The truck nanothorns resulted from the oriented aggregation based growth along the [010] direction with many steps on its surface, and the branch nanothorns were based on the normal growth along the [101] direction from the step station and exhibited a relative smooth surface.

IV. Conclusions

The nanostructured CPMs with tunable size of 100−200 nm to 4−6 μm have been fabricated by a simple solution method. The CPMs were built up with compressed nanothorns exhibiting tapering feature with tip size less than 10 nm. The tartrate anions should be responsible for the fabrication of CPMs, and the diameter of CPMs was significantly affected by the reactant concentration and could also be controlled by adjusting the molar ratio of NaOH to Cu^{2+} in the precursor solution.

The fabrication of CPMs went through the rapid nucleation of $Cu(OH)_2$, in situ dehydration of $Cu(OH)_2$ and the oriented-aggregation-based growth of CuO truck nanothorns simultaneously, and the normal crystal growth on the surface steps of CuO truck nanothorns. The reactant concentrations, especially the tartrate concentration, affected the fabrication mechanism. The formation of $Cu(OH)_2$ clusters was due to the releasing of Cu^{2+} and OH^- from $Cu(C_4H_2O_6)^{2-}$ anions upon heating, and the subsequent oriented-aggregation-based growth along [010] direction resulted from the coordinated or absorbed tartrate anions on the crystal surface. The final normal growth of CuO truck nanothorns along [101] direction caused by high free energy of the active cites on the steps of the truck nanothorn surface was controlled by the reversible reaction between $Cu(C_4H_2O_6)^{2-}$ and Cu^{2+} due to its much slower reaction rate. It was also the slower releasing rate of Cu^{2+} cations than the crystal growth rate and the larger supersaturation for nucleation than crystal growth that resulted in the successful separation of nucleation and crystal growth.

References and Notes

(1) Chen, S. H.; Fan, Z. Y.; Carroll, D. L. *J. Phys. Chem. B* **2002**, *106*, 10777. (b) Ewers, T. D.; Sra, A. K.; Norris, B. C.; Cable, R. E.; Cheng, C. H.; Shantz, D. F.; Schaak, R. E. *Chem. Mater.* **2005**, *17*, 514. (c) Yang, H. G.; Zeng, H. C. *Angew. Chem., Int. Ed. Engl.* **2004**, *43*, 5930. (d) Yang, X. J.; Makita, Y.; Liu, Z. H.; Sakane, K.; Ooi, K. *Chem. Mater.* **2004**, *16*, 5581.

(2) (a) Ma, Y. R.; Qi, L. M.; Ma, J. M.; Cheng, H. M. *Cryst. Growth Des.* **2004**, *4*, 351. (b) Chen, X. Y.; Wang, X.; Wang, Z. H.; Yang, X. G.; Qian, Y. T. *Cryst. Growth Des.* **2005**, *5*, 347. (c) Shi, H. T.; Qi, L. M.; Ma, J. M. Cheng, H. M. *J. Am. Chem. Soc.* **2003**, *125*, 3450. (d) Zhang, J.; Sun, L. D.; Yin, J. L.; Su, H. L.; Liao, C. S.; Yan, C. H. *Chem. Mater.* **2002**, *14*, 4172.

(3) Mann, S. *Angew. Chem., Int. Ed. Engl.* **2000**, *39*, 3392.

(4) Gao, F.; Lu, Q. Y.; Xie, S. H.; Zhao, D. Y. *Adv. Mater.* **2002**, *14*, 1537.

(5) (a) Jun, Y. W.; Lee, S. M.; Kang, N. J.; Cheon, J. *J. Am. Chem. Soc.* **2001**, *123*, 5150. (b) Lu, Q. Y.; Gao, F.; Zhao, D. Y. *Angew. Chem., Int. Ed. Engl.* **2002**, *41*, 1932. (c) Qin, A. M.; Fang, Y. P.; Ou, H. D.; Liu, H. Q.; Su, C. Y. *Cryst. Growth Des.* 10.1021/cg049736o. (d) Lu, Q. Y.; Gao, F.; Zhao, D. Y. *Nano Lett.* **2002**, *2*, 725.

(6) (a) Wu, C. Z.; Xie, Y.; Wang, D.; Yang, J.; Li, T. W. *J. Phys. Chem. B* **2003**, *107*, 13583. (b) Ohgi, H.; Maeda, T.; Hosono, E.; Fujihara, S.; Imai, H. *Cryst. Growth Des.* 10.1021/cg049644z. (c) Lou, X. W.; Zeng, H. C. *J. Am. Chem. Soc.* **2003**, *125*, 2697.

(7) (a) Jana, N. R.; Gearheart, L.; Murphy, C. J. *Adv. Mater.* **2001**, *13*, 1389. (b) Chen, J. Y.; Herricks, T.; Geissler, M.; Xia, Y. N. *J. Am. Chem. Soc.* **2004**, *126*, 10854. (c) Qu, L. T.; Shi, G. Q.; Wu, X. F.; Fan, B. *Adv. Mater.* **2004**, *16*, 1200.

(8) (a) Bigi, A.; Boanini, E.; Walsh, D.; Mann, S. *Angew. Chem., Int. Ed. Engl.* **2002**, *41*, 2163. (b) Yu, S. H.; Co1lfen, H.; Antonietti, M. *J. Phys. Chem. B* **2003**, *107*, 7396. (c) Yu, S. H.; Cölfen, H.; Xu, A. W.; Dong, W. F. *Cryst. Growth Des.* **2004**, *4*, 33. (d) Yu, S. H.; Antonietti, M.; Co1lfen, H.; Hartmann, J. *Nano Lett.* **2003**, *3*, 379.

(9) (a) Musa, A. O.; Akomolafe, T.; Carter, M. J. *Sol. Energy Mater. Sol. Cells* **1998**, *51*, 305. (b) Wu, M. K.; Ashburn, J. R.; Torng, C. J.; Hor, P. H.; Meng, R. L.; Gao, L.; Huang, Z. J.; Wang, Y. Q.; Chu, C. W. *Phys. Rev. Lett.* **1987**, *58*, 908. (c) Zheng, X. G.; Xu, C. N.; Tomokiyo, Y.; Tanaka, E.; Yamada, H.; Soejima, Y. *Phys. Rev. Lett.* **2000**, *85*, 5170. (d) Prabhakaran, D.; Subramanian, C.; Balakumar, S.; Ramasamy, P. *Phys. C* **1999**, *319*, 99. (e) Borgohain, K.; Mahamuni, S. *J. Mater. Res.* **2002**, *17*, 1220.

(10) (a) Maruyama, T. *Sol. Energy Mater. Sol. Cells* **1998**, *56*, 85. (b) Rakhshni, A. E. *Solid State Electron.* **1986**, *29*, 7.

(11) (a) Lanza, F.; Feduzi, R.; Fuger, J. *Mater. Res.* **1990**, *5*, 1739. (b) Gao, X. P.; Bao, J. L.; Pan, G. L.; Zhu, H. Y.; Huang, P. X.; Wu, F.; Song D. Y. *J. Phys. Chem. B* **2004**, *108*, 5547.

(12) (a) Lee, S. H.; Her, Y. S.; Matijevic, E. *J. Colloid Interface Sci.* **1997**, *186*, 193. (b) Chen, D.; Shen, G. Z.; Tang, K. Z.; Qian, Y. T. *J. Cryst. Growth* **2003**, *254*, 225. (c) Hong, Z. S.; Cao, Y.; Deng, J. F. *Mater. Lett.* **2002**, *52*, 34. (d) Yang, R.; Gao, L. *Chem. Lett.* **2004**, *33*, 1194. (e) Kumar, R. V.; Diamant, Y.; Gedanken, A. *Chem. Mater.* **2000**, *12*, 2301. (f) Liangy, Z. H.; Zhu, Y. J. *Chem. Lett.* **2004**, *33*, 1314.

(13) (a) Xu, C. K.; Liu, Y. K.; Xu, G. D.; Wang, G. G. *Mater. Res. Bull.* **2002**, *37*, 2365. (b) Cao, M. H.; Hu, C. W.; Wang, Y. H.; Guo, Y. H.; Guo, C. X.; Wang, E. B. *Chem. Commun.* **2003**, 1884.

(14) (a) Chang, Y.; Zeng, H. C. *Cryst. Growth Des.* **2004**, *4*, 397. (b) Zhu, C. L.; Chen, C. N.; Hao, L. Y.; Hu, Y.; Chen, Z. Y. *J. Cryst. Growth* **2004**, *263*, 473. (c) Zhu, C. L.; Chen, C. N.; Hao, L. Y.; Hu, Y.; Chen, Z. Y. *Solid State Commun.* **2004**, *130*, 681. (d) Lu, C. H.; Qi, L. M.; Yang, J. H.; Zhang, D. Y.; Wu, N. Z.; Ma, J. M. *J. Phys. Chem. B* **2004**, *108*, 17825. (e) Song, X. Y.; Sun, S. X.; Zhang, W. M.; Yu, H. Y.; Fan, W. L. *J. Phys. Chem. B* **2004**, *108*, 5200. (f) Du, G. H.; Van Tendeloo, G. *Chem. Phys. Lett.* **2004**, *393*, 64. (g) Gao, X. P.; Bao, J. L.; Pan, G. L.; Zhu, H. Y.; Huang, P. X.; Wu, F.; Song, D. Y. *J. Phys. Chem. B* **2004**, *108*, 5547. (h) Hou, H. W.; Xie, Y.; Li, Q. *Cryst. Growth Des.* **2005**, *5*, 201.

(15) Zhao, Y.; Zhu, J. J.; Hong, J. M.; Bian, N. S.; Chen, H. Y. *Eur. J. Inorg. Chem.* **2004**, 4072.

(16) Zhang, L. Z.; Yu, J. C.; Xu, A. W.; Li, Q.; Kwong, K. W.; Yu, S. H. *J. Cryst. Growth* **2004**, *266*, 545.

(17) Liu, B.; Zeng, H. C. *J. Am. Chem. Soc.* **2004**, *126*, 16744.

(18) (a) Luo, T. J. M.; MacDonald, J. C.; Palmore, G. T. R. *Chem. Mater.* **2004**, *16*, 4916. (b) Penn, R. L. *J. Phys. Chem. B* **2004**, *108*, 12707. (c) Oliveira, A. P. A.; Hochepied, J. F.; Grillon, F.; Berger, M. H. *Chem. Mater.* **2003**, *15*, 3202.

(19) Nakamoto, K. *Infrared Spectra of Inorganic and Coordination Compound* (in Chinese); Huang, D., Wang, R., Translators; 4th Chemical Industry Press: Beijing, 1991; p 251.

(20) Nakamoto, K. (*Infrared Spectra of Inorganic and Coordination Compound* (in Chinese); Huang, D., Wang, R., Translators; 4th Chemical Industry Press: Beijing, 1991; p 237.

(21) Nyquist, R. A.; Kagel, R. O. *Infrared Spectra of Inorganic Compounds*; Academic Press: New York and London, 1971; p 220.

(22) (a) Cotton, F. A.; Wise, J. J. *Inorg. Chem.* **1967**, *6*, 917.

(23) Chen, S. C.; Tang, C. Y.; Ding, Z. D. *Important Inorganic Reaction* (in Chinese); Science and Technology Press of Shanghai: Shanghai, 1994; p 1351.

(24) Penn, R. L.; Banfield, J. F. *Science* **1998**, *281*, 969.

(25) Kuz'menko, A. B.; Marel, D. V.; Bentum, P. J. M. V.; Tishchenko, E. A.; Presura, C.; Bush, A. A. *Phys. Rev. B* **2001**, *63*, 094303.

(26) (a) Peng, X. G. *Adv. Mater.* **2003**, *15*, 459. (b) Lee, S. M.; Cho, S. N.; Cheon, J. *Adv. Mater.* **2003**, *15*, 441.